World Journal of Microbiology and Biotechnology (2022) 38: 186
https://doi.org/10.1007/s11274-022-03365-7

ORIGINAL PAPER

Mitigating the toxicity of palmitoylated analogue of α-melanocyte stimulating hormone(11–13) by conjugation with gold nanoparticle: characterisation and antibacterial efficacy against methicillin sensitive and resistant *Staphylococccus aureus*

Sayani Mitra[1] · **Aftab Hossain Mondal**[1,2] · **Kasturi Mukhopadhyay**[1]

Received: 14 January 2022 / Accepted: 25 July 2022 / Published online: 16 August 2022

Abstract
In an attempt to develop potent and non-toxic antimicrobial agent, the palmitoylated analogue of α-melanocyte stimulating hormone(11–13), Pal-α-MSH(11–13) was conjugated with gold nanoparticles (GNPs) for the first time and the efficacy of derived complex was investigated against two strains of *Staphylococccus aureus*. The GNPs were synthesized using tri-sodium citrate as reductant and Pal-α-MSH(11–13) was conjugated thereafter. The particles were characterised by UV-vis spectroscopy, transmission electron microscopy, dynamic light scattering, fourier transform infrared spectroscopy etc. Conjugation occurred via electrostatic interaction between anionic GNPs and cationic Pal-α-MSH(11–13). The zeta potential of GNP-Pal-α-MSH(11–13) was − 26.91, indicating its stability. The antibacterial activity was determined by minimal inhibitory concentration (MIC) and killing kinetics assay, whereas, inhibition of biofilm formation was studied by determining the biofilm biomass by crystal violet dye binding method, viability of biofilm-embedded cells by counting CFUs and metabolic activity by MTT (3-(4,5-dimethylthiazol-2-yl)-2,5-diphenyltetrazolium bromide) assay. The toxicity was analysed by hemolysis assay against murine RBCs and cytotoxicity against 3T3 fibroblasts. The MIC was 18 µM for GNP-Pal-α-MSH(11–13) and 12 µM for Pal-α-MSH(11–13). The killing kinetics and biofilm inhibition studies indicated the comparable efficacy of peptide before and after nano-conjugation. Importantly, the conjugation resulted in diminished toxicity, as evidenced by 0.29 ± 0.03% hemolysis and 100% viable fibroblasts at 72 µM compared to the Pal-α-MSH(11–13), showing 74.99 ± 1.59% hemolysis and 59.39 ± 1.06% viable fibroblasts. The nano-fabrication drastically reduced the peptide toxicity without compromising its antibacterial efficacy. The anionicity of the conjugate may be responsible for non-toxicity that makes them suitable for pharmaceutical applications.

Keywords α-Melanocyte stimulating hormone · Gold nanoparticles · *Staphylococcus aureus* · Biofilm · Cytotoxicity

Introduction

Antimicrobial resistance (AMR) has been considered as one of the major global threat for human health and development, as declared by World Health Organization (WHO). Since the last two decades, the misuse of antibiotics and the emergence of different drug resistant bacterial variants have boosted the escalating occurrence of AMR (Ferri et al. 2017). Furthermore, the manifestation of four viral outbreaks i.e. SARS-CoV epidemic (2002), the H1N1 pandemic (2009), Middle East Respiratory Syndrome (MERS) outbreak (2012), and finally the COVID-19 pandemic (2019) have fuelled up the overusage/ misusage of antimicrobials to combat secondary bacterial infections, thereby are now promoting the outgrowth of AMR pattern worldwide (Manohar et al. 2020). Under the current circumstances, it is highly necessary to modify the usual method of antibiotic therapy and develop alternative antimicrobial

✉ Kasturi Mukhopadhyay
kasturim@mail.jnu.ac.in

[1] Antimicrobial Research Laboratory, School of Environmental Sciences, Jawaharlal Nehru University, 110067 New Delhi, India

[2] Present address: Department of Microbiology, Faculty of Allied Health Sciences, Shree Guru Gobind Singh Tricentenary University, Gurugram-122505 Haryana, India

agents. A promising approach to tackle antibiotic crisis amid rapidly increasing AMR, is the application of antimicrobial peptides (AMPs), that represent a significant class of antimicrobials and are widely distributed in nature as part of host immune defence systems of different organisms including microbes, plants, mammals, insects etc. (Mahlapuu et al. 2016; Huan et al. 2020). Cationic AMPs are considered as a potential source of future antimicrobials because of their various advantageous features like low tendency for resistance development and broad spectrum activity against a variety of microorganisms.

Staphylococcus aureus is considered as an important human pathogen that causes different clinical infections like soft tissue or skin infections, endocarditis, bacteremia and device-related infections (Tong et al. 2015). Since the last two decades, this organism is also considered as one of the prominent pathogens for healthcare as well as community associated infections, contributing to mortality and morbidity, due to their incredible ability to acquire AMR. Starting from the introduction of penicillin in 1940s to the methicillin in 1960s, emergence of methicillin resistant *S. aureus* (MRSA) strains in late 1970s followed by the rise of vancomycin-resistant *S. aureus* (VRSA) strains in 2002, the World has observed a total of four epidemic waves till date (Chambers and DeLeo, 2009). The most commonly known nosocomial organism responsible for catheter associated infections is *S. aureus*, which has natural affinity to attach to catheter surfaces (Trautner and Darouiche 2004). *S. aureus* adhesion to medical implants and host tissue followed by the biofilm formation, is the causative factor for chronic infections. The establishment of biofilm, along with EPS formation, decreases the susceptibility to antimicrobials, thereby increasing complications for the biofilm associated infections (Lister and Horswill 2014). According to WHO data, drug resistant strains of *S. aureus* and *Escherichia coli* caused more than 2.6 lakh cases of blood stream infections and 8,200 casualties in European countries in 2007, which led to the healthcare expense of € 62 million (Ferri et al. 2017).

Of interest, α-melanocyte stimulating hormone (α-MSH) is an anti-inflammatory peptide comprising of 13 amino acids, that is produced by different cell types such as keratinocytes, monocytes, endothelial cells etc. Based on the significant similarities with natural AMPs, the antimicrobial activities of α-MSH have been explored over the last decade, and the whole peptide as well as its C-terminal region [namely α-MSH(6–13) and α-MSH(11–13)] were reported to be active against various microorganisms including *Candida albicans, E. coli, S. aureus* etc. (Catania et al. 2005; Charnley et al. 2008; Singh and Mukhopadhyay 2011). Mukhopadhyay and her research group have been pursuing antibacterial properties of α-MSH and its various analogues with rapid and strong efficacy against *S. aureus* including MRSA (Singh and Mukhopadhyay 2011, 2014; Shireen et al. 2012; Singh et al. 2016, 2020; Mumtaz et al. 2020) and *E. coli* (Tiwari et al. 2022).

Despite having negligible cytotoxicity, the parent peptide, α-MSH has physiological limitations like reduced activity in presence of bacterial growth media, that affects their therapeutic potential. Grieco et al. (2013) designed a number of novel analogues replacing Gly10 in the DNal sequence with natural and unnatural amino acids, showing broad spectrum antimicrobial action in standard microbiological culture conditions. Moreover, recently designed analogue by Singh et al. (2020), Ana-5 was found to exhibit strong staphylocidal potential in presence of both growth media and serum with ex vivo efficacy and very nominal toxicity, representing their high therapeutic aptitude. Previously, Several researchers reported that C-terminal amino acid sequences of α-MSH, α-MSH(6–13) and α-MSH(11–13) exhibited rapid antimicrobial efficacy which is equivalent to that of the parent peptide, while α-MSH(6–9) was responsible for melanogenic activity (Catania et al. 2005; Charnley et al. 2008; Singh and Mukhopadhyay 2011). It is significant to state that the shortest C-terminal sequence [Lys-Pro-Val or α-MSH(11–13)] contributes to both anti-inflammatory and antibacterial activity, rendering it as the potent therapeutic agent. Therefore, α-MSH(11–13) may be of high interest to be taken for further structural modification to make it active in standard culture environment and extending their clinical potential. In a parallel study, the N-terminal palmitoylation in α-MSH(11–13), resulted in exhibiting efficacy in bacterial growth media with rapid killing action against *S. aureus* (Mumtaz et al. 2020).

Alteration in membrane permeability and interference with DNA replication/protein synthesis inhibition were found to be responsible for efficacy of α-MSH against *S. aureus* (Singh and Mukhopadhyay 2011). Recently, it has been observed that enhanced cationicity of the designed α-MSH analogues exhibited increased staphylocidal efficacy and membrane damaging activity without compromising the host cell selectivity, due to the increased electrostatic interactions between the peptides and negatively charged bacterial membranes (Singh et al. 2016). Charnley et al. (2008) also confirmed the antibacterial activity of C-terminal region of α-MSH (i.e., Ac-Lys-Pro-D-Val-NH_2 and Ac-Lys-Pro-Val-NH_2) against *E. coli*. Some novel analogue designed by Mukhopadhyay and her research group, by substituting the sequence of α-MSH(6–13) with arginine and tryptophan residues, was found to be highly active against *S. aureus* cultures grown in bacterial growth media (Singh et al. 2020), though the parent peptide and its derivatives, reported earlier were active only in presence

of physiological buffers (Singh and Mukhopadhyay 2011; Shireen et al. 2012).

The research had been further extended by the successful design of N-terminal palmitoylated analogue of α-MSH(11–13), that was not only active in growth media, but also exhibited potent staphylocidal activity against both planktonic cells and biofilm (Mumtaz et al. 2020). The novel analogue, Pal-α-MSH(11–13) was membrane active similar to the parent peptide, and inhibited stationary phase cells as well as the biofilm development by both methicillin sensitive *S. aureus* (MSSA) and MRSA. Moreover, AMR was not developed in MRSA cells upon treatment with 18 serial passages at sub-MIC of the palmitoylated analogue.

Some CAMPs exhibit toxicity toward eukaryotic cells, that might be less applicable for clinical applications. A potential attempt to diminish the cytotoxicity can be feasible via nanofabrication and conjugation with GNPs (Rajchakit and Sarojini 2017). Therefore, it is necessary to modify the research goals and functionalize the toxic AMPs using the nano-carriers like GNPs, to increase their cell-selectivity as well as for subsequent drug release over an extended period. The antimicrobial drug coating on GNP surfaces promote the delivery and subsequent release of the drug molecules to exhibit potent antibacterial activity (Yougbare et al. 2019). Over the past few years, citrate reduced GNPs have been used for AMP conjugation with a hope to enhance its bactericidal efficacy and develop stable and non-toxic nano-AMP therapeutics (Casciaro et al. 2017; Lee et al. 2017; Yeom et al. 2016). Despite possessing an excellent staphylocidal potential, Pal-α-MSH(11–13) exerted little cytotoxicity at tested concentrations against mammalian cells (Mumtaz et al. 2020), which might be concentration dependent and may loose cell selectivity at higher concentrations (may be needed to treat other strains). Therefore, the motivation of the current study came up with a new hope to diminish the cytotoxicity of Pal-α-MSH(11–13) by GNP conjugation for the first time, without hampering its bactericidal activity against *S. aureus*.

Materials and methods

Materials

The customized synthesis of the peptide Pal-α-MSH(11–13) was done by BioChain Incorporated, India. Chloroauric acid ($HAuCl_4$), Tri-sodium citrate ($Na_3C_6H_5O_7$), 3-(4,5-dimethylthiazol-2-yl)-2,5-diphenyltetrazolium bromide (MTT), crystal violet (CV), melittin, Dulbecco's modified Eagle's medium (DMEM), Triton X-100, dimethyl sulfoxide (DMSO) were obtained from Sigma-Aldrich (USA). Fetal bovine serum (FBS) was obtained from Gibco, India. The bacterial culture media cation-adjusted Mueller-Hinton Broth (MHB), tryptic soy broth (TSB), brain heart infusion (BHI) broth/agar and standard antibiotics were obtained from Himedia (India).

Two bacterial strains, methicillin-sensitive *S. aureus* ATCC 29213 (MSSA) and methicillin-resistant *S. aureus* ATCC 33591 (MRSA) were used in the current study.

Synthesis of gold nanoparticles

Gold nanoparticles (GNPs) were synthesized by tri-sodium citrate as reducing agent according to Turkevich/Frens method (Turkevich et al. 1951; Frens 1973). Briefly, 50 ml of 0.02% chloroauric acid was boiled on a hot-plate for 10 min after which 1 ml of tri-sodium citrate (0.5 mg/ml) was added followed by heating for 15 min. The resulting wine-red coloured solution was stored at 4 °C. The concentration of GNP solution was determined spectrophotometrically at 526 nm ($\varepsilon = 2.33 \times 10^8$ M^{-1} cm^{-1}) (Baptista et al. 2005).

Synthesis of peptide conjugated GNPs

The Pal-α-MSH(11–13) conjugated GNPs [GNP-Pal-α-MSH(11–13)] was synthesized following Singh et al. 2017 with brief modifications. The GNPs and the peptide were mixed in a ratio of 1.9 nM: 600 nM followed by overnight incubation at 10 °C with shaking at 100 rpm. Before that, the GNP : peptide ratio was optimized over a broad range to avoid any visible clumping and precipitation of particles (Fig. S1 of Supplementary Information). Highest concentration of the Pal-α-MSH(11–13) with 1.9 nM GNPs, which yielded no visible precipitation of the nanoparticles, was considered as the optimal conjugation and taken for further analysis. The colour of the reaction mixture involving GNP : peptide ratio of 1.9 nM: 600 nM changed from red to blue with no particle aggregation, indicating the successful completion of the reaction. The peptide conjugated GNPs were washed twice with sterile de-ionised water by centrifuging at 12,000 rpm for 20 min to remove the free peptides and stored at 4 °C for further use.

Characterisation of nanoparticles

UV-Visible spectroscopy

The GNPs and GNP-Pal-α-MSH(11–13) were analyzed by UV-Visible spectroscopy (UV-2450 Spectrophotometer, Shimadzu) by recording the absorbance spectra in the range from 400 to 800 nm with a resolution of 1 nm. A difference in the peak absorption (λ_{max}) between the spectra of unconjugated and peptide conjugated GNPs may indicate

the successful peptide conjugation onto the GNP surfaces (Singh et al. 2017).

Dynamic light scattering and zeta potential

Hydrodynamic diameter and size distribution of the nanoparticles was measured by dynamic light scattering (DLS) (3D LS Spectrometer, LS Instruments) at following parameters; Scattering angle: 90°, Duration (s): 30, Wavelength (nm): 632, Temperature (K): 298.0, Laser intensity (mW): 0.25. Zeta potential of the unconjugated GNPs, Pal-α-MSH(11–13) and GNP-Pal-α-MSH(11–13) were determined by zeta potential analyzer (Zeecom ZC-3000, Microtec Co.).

Transmission electron microscopy and selected area electron diffraction

The nanoparticles were further characterised by transmission electron microscopy (TEM) for the determination of shape and size. For this, the samples were dried on carbon-coated copper grids and then put for TEM analysis at 200 kV (JEOL 2100 F) (Manson et al. 2011). The selected area electron diffraction (SAED) patterns of the particles were also taken by the same instrument.

Fourier transform infrared spectroscopy

The fourier transform infrared spectroscopy (FTIR) was performed to identify the surface functionalization and confirm the presence of the peptide over GNP surfaces. Infrared spectra were collected by drop-casting 2 µl aliquot of each sample and the spectra was recorded at a resolution of 2 cm^{-1} over a wavenumber range of 600–4000 cm^{-1} (Tensor 37, Bruker) (Bonor et al. 2014; Mondal et al. 2020).

Thermogravimetric analysis

Thermogravimetric analysis (TGA) was performed in the instrument TGA1 (Mettler Toledo, India) combined with Minichiller MT/230 and STARe software V13.00 (Payne et al. 2016), to determine the amount of Pal-α-MSH(11–13) conjugated with the GNPs, hence the conjugation efficiency (%). Briefly, the Pal-α-MSH(11–13) and GNP-Pal-α-MSH(11–13) were lyophilized overnight and ~2 mg of both was heated separately over the temperature range of 25 to 800 °C for the analysis. The amount of peptide conjugation was calculated as the percentage weight loss or degradation of the GNP-Pal-α-MSH(11–13) at this temperature range.

Minimal inhibitory concentration and minimal bactericidal concentration

Minimal inhibitory concentration (MIC) of conjugated and unconjugated Pal-α-MSH(11–13) were determined against both MSSA (ATCC 29213) and MRSA (ATCC 33591) by standard broth microdilution assay as per the guidelines of the Clinical and Laboratory Standards Institute (CLSI) (CLSI, 2018). Briefly, after overnight growth of *S. aureus* at 37 °C, the cell suspensions were centrifuged and cell density was adjusted in cation adjusted MHB, to OD_{600} of ~ 0.5 (corresponds to ~ 10^8 CFU/mL). The test solutions were diluted using 2-fold serial dilution in the same medium. A final of 5×10^5 CFU/mL bacterial cell density was used in each well of the 96- well microtitre plate. The plates also contained column for negative control (with only media) and growth control (with only cells). The plates were incubated for 16–18 h at 37 °C. The MIC value was determined as the lowest concentration of the agents that gave no visible turbidity in the well, hence inhibited the bacterial growth.

To determine the MBC, the suspension was taken starting from the 1st well upto the MIC well and streaked onto the BHI plates. After incubated overnight at 37 °C, the minimum concentration producing no colony on agar plates was considered as the MBC, that completely killed the bacteria (Mondal et al. 2020). The experiment was performed twice independently in duplicates.

Tolerance level

The tolerance level of the bacteria indicates the bacteriostatic or bactericidal action of the tested agent. Here, the tolerance level of MSSA (ATCC 29213) and MRSA (ATCC 33591) was estimated against the GNP-Pal-α-MSH(11–13) using the following formula (May et al. 1998; Mondal et al. 2020).

Tolerance = MBC/MIC.

The above ratio greater than 16 considers the test agent as bacteriostatic, while the same less than 4 considers the agent to possess bactericidal activity (Mohammed et al. 2018).

Antibacterial kinetics

The antibacterial potency was compared between the Pal-α-MSH(11–13) and GNP-Pal-α-MSH(11–13) by studying the killing kinetics in TSB against stationary phase cells of *S. aureus* following standard drop plate method (Singh et al. 2016; Mumtaz et al. 2020). To describe briefly, stationary phase culture of *S. aureus* was centrifuged to get the cell pellet. The cells were resuspended in fresh TSB and diluted to the desired cell densities (considering OD_{600} of ~ 0.5 corresponds to ~ 10^8 CFU/mL). After that, the cells

were treated with different concentrations of test agents at 37 °C with 180 rpm. At various time points, aliquots were taken, diluted and 15 µL of each dilution was plated on agar plates. Bacterial colony forming units (CFU) were counted after 16–18 h incubation at 37 °C and the cell numbers of the treated plates were compared with that of the untreated control. The mean ± standard deviation (SD) for viable cells was represented in terms of Log_{10} CFU/mL. The experiment was performed twice independently in duplicates.

Biofilm susceptibility

Biofilm susceptibility assays were performed by CV staining for studying the inhibition of biofilm biomass and MTT assay for evaluating the biofilm viability (Traba and Liang 2011). The cell viability of the biofilm was also determined by the colony count, as described by Joshi et al. (2018).

For the biofilm formation, overnight grown MRSA (ATCC 33591) (considering OD_{600} of ~ 0.5 corresponds to ~ 10^8 CFU/mL) was diluted in fresh TSB to the desired cell concentration (10^5 CFU/mL). 100 µL of this cell suspension was added to each well of a polystyrene 96-well plate, and the biofilm was allowed to grow in static condition for 24 h at 37 °C in the presence of desired concentration of the test agents. The growth control wells did not have any compound, whereas the negative control wells contained 100 µL of sterile media. After 24 h, CV staining and MTT assay were performed to evaluate the biofilm inhibition.

In CV staining, after allowing the biofilms to grow for 24 h in microtitre plate, the spent media was removed, and the wells were washed twice with 10 mM PBS (pH 7.4) gently to discard the non-adherent planktonic cells. Then, the biofilms were fixed for 1 h at 60 °C and stained with 125 µL of 0.1% aqueous CV for 20 min. The wells were then washed with PBS twice to remove the unbound CV and air-dried for 5 min at room temperature. The dye attached to the biofilm biomass was then dissolved in 125 µL of 33% glacial acetic acid. The microtitre plate was read at 570 nm using microplate reader (Molecular Devices, Sunnyvale, CA, USA) to quantify the biofilm biomass.

For MTT assay, the wells of the 96-well microtitre plate containing the biofilms were washed twice with 200 µL of 10 mM PBS (pH 7.4) gently. The biofilms were treated with 100 µL of 0.5 mg/mL MTT, and incubated at 37 °C for 2 h in dark. After removing the MTT from each well, 200 µL DMSO were added and incubated further at 37 °C for 10–15 min in dark. 100 µL of this suspension was transferred from each well to a fresh plate and absorbance was read at 570 nm using microplate reader (Molecular Devices, Sunnyvale, CA, USA).

To determine the number of viable cells within the biofilm, the wells were first washed with 200µL PBS to discard the planktonic cells, followed by the addition of 100 µL PBS to each well. The wells were then scraped thoroughly, cell suspensions were bath-sonicated at 40 kHz for 5 min and plated onto BHI plates. After incubation for 16 – 18 h at 37 °C, the CFUs were counted and the mean ± SD for viable cells was represented in terms of Log_{10} CFU/mL. These experiments were performed twice independently in duplicates.

Hemolytic activity

The hemolytic activity was determined against mice red blood cells following Singh et al. 2016. Briefly, fresh murine red blood cells (RBCs) were washed with 35 mM PBS (pH 7.4) by centrifugation at 1500 rpm for 10 min. The pellet of RBCs was resuspended in 4% (v/v) in the same buffer. Two-fold serial dilutions of test agents (100 µL) were prepared in 96-well microtitre plates to which 100 µL of 4% (v/v) RBC suspensions were added and incubated at 37 ºC for 1 h. The hemoglobin release was obtained by centrifuging the plates at 1500 rpm and measuring OD at 414 nm. Wells treated with 0.1% Triton X-100 were considered as positive control (100% hemolysis), and untreated RBCs were considered as negative control. The percentage of hemolysis was determined as shown below. The experiment was performed twice independently in duplicates.

$$\%\text{Hemolysis} = \frac{\text{OD of Sample} - \text{OD of PBS}}{\text{OD of 0.1\% TritonX} - \text{OD of PBS}} \times 100$$

For hemolysis experiment, the guidelines of CPCSEA (Committee for the Purpose of Control and Supervision of Experiments on Animals) were followed and performed on approval by Institutional Animal Ethics Committee (IAEC-17/2019) of Jawaharlal Nehru University, New Delhi, India.

Cytotoxicity

The cytotoxicity of the Pal-α-MSH(11–13) and GNP-Pal-α-MSH(11–13) was studied by MTT assay against mammalian 3T3 fibroblast cell line (Singh et al. 2013; Mumtaz et al. 2020). Briefly, the cells were seeded into 24-well plates at 20,000 cells/well (determined by trypan blue staining method) in DMEM (containing 10% FBS) for 24 h. After 75% confluent growth (refers to the 75% coverage of the wells by the cells, determined visually by inverted microscopy), the cells were treated with desired concentrations of the test agents dissolved in DMEM (without FBS), and incubated in 5% CO_2 incubator for 2 h at 37 °C. After the wells were washed with PBS, 1 mL of 0.1 mg/mL MTT (dissolved in DMEM) was added, and the plate was incubated in dark for 2 h (5% CO_2 at 37 °C). After that, each well was treated

with 200 µL of DMSO to lyse the cells and dissolve the purple coloured formazan crystals. 150 µL of this solution was transferred from each well to a fresh 96-well plate and the absorbance was read at 570 nm using microplate reader (Molecular Devices, Sunnyvale, CA, USA). Triplicate wells without treatment and wells treated with 2% Triton X-100 were considered as growth control and positive control, respectively. The cytotoxicity was presented as the percentage survival of cells relative to growth control calculated as shown below (Joshi et al. 2018). The experiment was performed twice independently in triplicates.

$$\% \text{ Survival of cells} = \frac{\text{OD of sample}}{\text{OD of growth control}} \times 100$$

Statistical analysis

All the experiments were performed twice independently on different days in duplicates or triplicates and mean ± SD were calculated using Prism 8 program (GraphPad Software Inc., La Jolla, CA, USA).

Results

Proposed mechanism of synthesis of GNP-Pal-α-MSH(11–13)

The amino acid sequences and chemical structures of the parent peptide α-MSH and analogues, α-MSH(11–13) and Pal-α-MSH(11–13) are given in the Table S1 of the Supplementary Information. The GNPs were synthesized using tri-sodium citrate, that provided them the negative charge to be suitable for conjugation with the positively charged peptide Pal-α-MSH(11–13). Here the nano-fabrication was done using tri-sodium citrate as the reducing agent and Pal-α-MSH(11–13) as capping agent (Fig. S2 of Supplementary Information).

Characterisation of GNP and GNP-Pal-α-MSH(11–13)

UV-Vis spectra were taken from 400 to 800 nm, that showed a strong absorption peak at 526 nm for GNPs (red line) while the λ_{max} was shifted to 632 nm for GNP-Pal-α-MSH(11–13) (blue line). The shifting in peak was due to change in surface chemistry in nanoparticles after peptide addition, indicating the successful conjugation (Fig. 1a). The physical appearance of GNP-Pal-α-MSH(11–13) was blue in color, while the GNP was wine red (Fig. 1b and c). DLS and TEM analysis revealed the hydrodynamic diameter and average particle

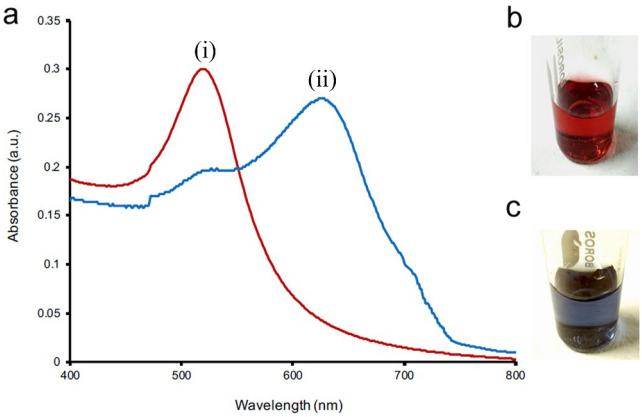

Fig. 1 (a) UV-Vis spectroscopic analysis of GNP (i) and GNP-Pal-α-MSH(11–13) (ii) showing absorption peak at 526 and 632 nm respectively, Physical appearance of (b) GNP and (c) GNP-Pal-α-MSH(11–13)

Table 1 Characterization of synthesized nanoparticles

	λ_{max} (nm)	Average diameter from TEM (nm)	Hydrodynamic diameter from DLS (nm)	Zeta potential (mV)
GNP	526	11.94 ± 1.8	23.71 ± 4.21	-40.36
GNP-Pal-α-MSH(11–13)	632	11.9 ± 1.05	172.99 ± 15.89	-26.91

diameter for the unconjugated GNPs as 23.71 ± 4.21 nm and 11.94 ± 1.8 nm, respectively (Table 1; Fig. 2a and e). The nanoparticles were mostly spherical in shape, as observed in TEM. No difference was obtained in the particle sizes after peptide conjugation, which were found to be 11.9 ± 1.05 nm for GNP-Pal-α-MSH(11–13) conjugate, as obtained by TEM analysis (Fig. 2b). This was expected, as the gold core is only visible at the acceleration voltage used in TEM (Hall et al. 2007; Manson et al. 2011). However, the hydrodynamic diameter increased to 172.99 ± 15.89 nm upon peptide addition, as obtained by DLS technique, that was sensitive to the peptide conjugation(Table 1; Fig. 2f). The crystalline nature of the nanoparticles was investigated by SAED. The SAED patterns of GNP (Fig. 2c) and GNP-Pal-α-MSH(11–13) (Fig. 2d) showing the diffractions from the (111), (200), (220) and (311) reflection planes of the face centred cubic (fcc) of gold. The inter-planar d-spacing of bare GNP was found to be 2.32 Å and that of the peptide-conjugate was 2.26 Å corresponding to the (111) lattice plane of gold. The values calculated from the SAED data were confirmed by high resolution TEM analysis. Our results were supportive of the data obtained by Suvarna et al. (2017), who reported the d-spacing of 2.36 Å for citrate capped spherical GNPs. Overall, the peptide conjugation was found not to affect the lattice configuration of the gold crystals, as observed by their analogous spectra and inter-planar spacing.

The FTIR spectrum of GNPs was shown in Fig. 3a. The characteristic peaks at 1400 cm^{-1} and 1647 cm^{-1} correspond

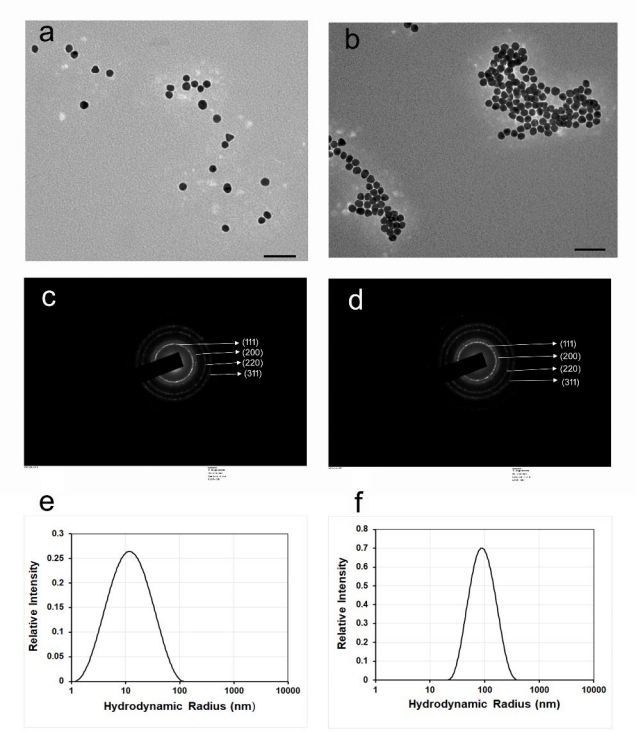

Fig. 2 Transmission electron microscopy images, SAED patterns and particle size distribution plots of (a, c and e) GNP and (b, d and f) GNP-Pal-α-MSH(11–13) respectively. Scale bar 50 nm

to the symmetric and anti-symmetric stretching of COO^- group, confirming the successful reduction by citrate and synthesis of GNPs. The FTIR spectrum of GNP-Pal-α-MSH(11–13) showed bands at 1600–1700 cm^{-1} (indicative of C = O, C-N stretch) (Fig. 3 d and e), that suggested the peptide capping over GNP surface (Wangoo et al. 2008). Peaks at 1340–1350 cm^{-1} in Pal-α-MSH(11–13) indicates the $-NH_2$ vibration of lysine (Fig. 3b and c) (Bonor et al. 2014), which were absent in the spectra of GNP-Pal-α-MSH(11–13). This phenomenon suggested that conjugation might occur via electrostatic interaction between negatively charged $-COO^-$ group on GNPs and secondary $-NH_3^+$ group of lysine residues in Pal-α-MSH(11–13). The average zeta potential of GNPs was −40.36 mV before conjugation. The zeta potential of Pal-α-MSH(11–13) was found to be +31.73 mV, that was responsible for partial neutralization of surface charge in the GNP-Pal-α-MSH(11–13) conjugate, the value of which was recorded as -26.91 mV(Table 1, Fig. S3 of Supplementary Information). The zeta data showed high colloidal stability of the synthesized nanoparticles and indicated the electrostatic interaction between the peptide and GNPs. The TGA analysis was extremely essential to calculate both the mass and the concentration of the peptide bound to the GNP surfaces, needed for further experiments. The TGA spectra of Pal-α-MSH(11–13) showed the sharp weight loss in the temperature range of 200°–450 °C and then caused subsequent mass loss of 100% over the range up to 800 °C. The peptide conjugate showed analogous pattern, where rapid weight loss occurred in the range of 200°–500 °C, finally resulted in the weight loss of 4.85% over the whole range. The comparable spectral pattern of Pal-α-MSH(11–13) and GNP-Pal-α-MSH(11–13) confirmed the conjugation process (Fig. 4). The TGA data revealed the amount of the peptide conjugated with GNPs, which was about 3.05% by weight, from which the conjugation efficiency was calculated as 75% (SI1 of Supplementary Information).

Minimal inhibitory concentration and minimal bactericidal concentration

Previous studies showed, though the parent peptide α-MSH and its analogues did not exhibit any antibacterial activity in presence of standard bacterial growth media (Singh and Mukhopadhyay 2011; Singh et al. 2013, 2016, 2020), the palmitoylation on the α-MSH(11–13) enabled to retain its anti-staphylococcal efficacy in growth media like MHB and TSB (Mumtaz et al. 2020). Therefore, the MIC and MBC were determined to see the difference in their antibacterial potency (if any) between the peptide and peptide conjugated GNPs. The MIC as well as the MBC of GNP-Pal-α-MSH(11–13) and Pal-α-MSH(11–13) were 18 µM (~ 10.44 µg/ml) and 12 µM (~ 6.96 µg/ml) respectively against both MSSA (ATCC 29213) and MRSA (ATCC 33591) (Table 2). The unconjugated GNP did not show any cell inhibition at corresponding concentration needed for the synthesis of the conjugate GNP-Pal-α-MSH(11–13). Therefore, the MIC of the conjugate represents the concentration of the peptide [based on the molecular mass of Pal-α-MSH(11–13)] present in the nanoparticles. The standard antibiotic vancomycin exhibited a MIC of 0.75 µM (~ 1.11 µg/ml) against both the strains, while the MBC was found to be 1.5 µM (~ 2.22 µg/ml) against the MSSA (Table 2).

Tolerance level

The tolerance level of both tested strains against the GNP-Pal-α-MSH(11–13) and Pal-α-MSH(11–13) were calculated as 1, because of the identical MIC and MBC values. This data indicated the bactericidal properties of the tested agents (Mondal et al. 2020).

Antibacterial kinetics

The antibacterial kinetics was performed to compare the bactericidal potency between the peptide and peptide conjugated GNPs. Stationary phase cells of MSSA and MRSA

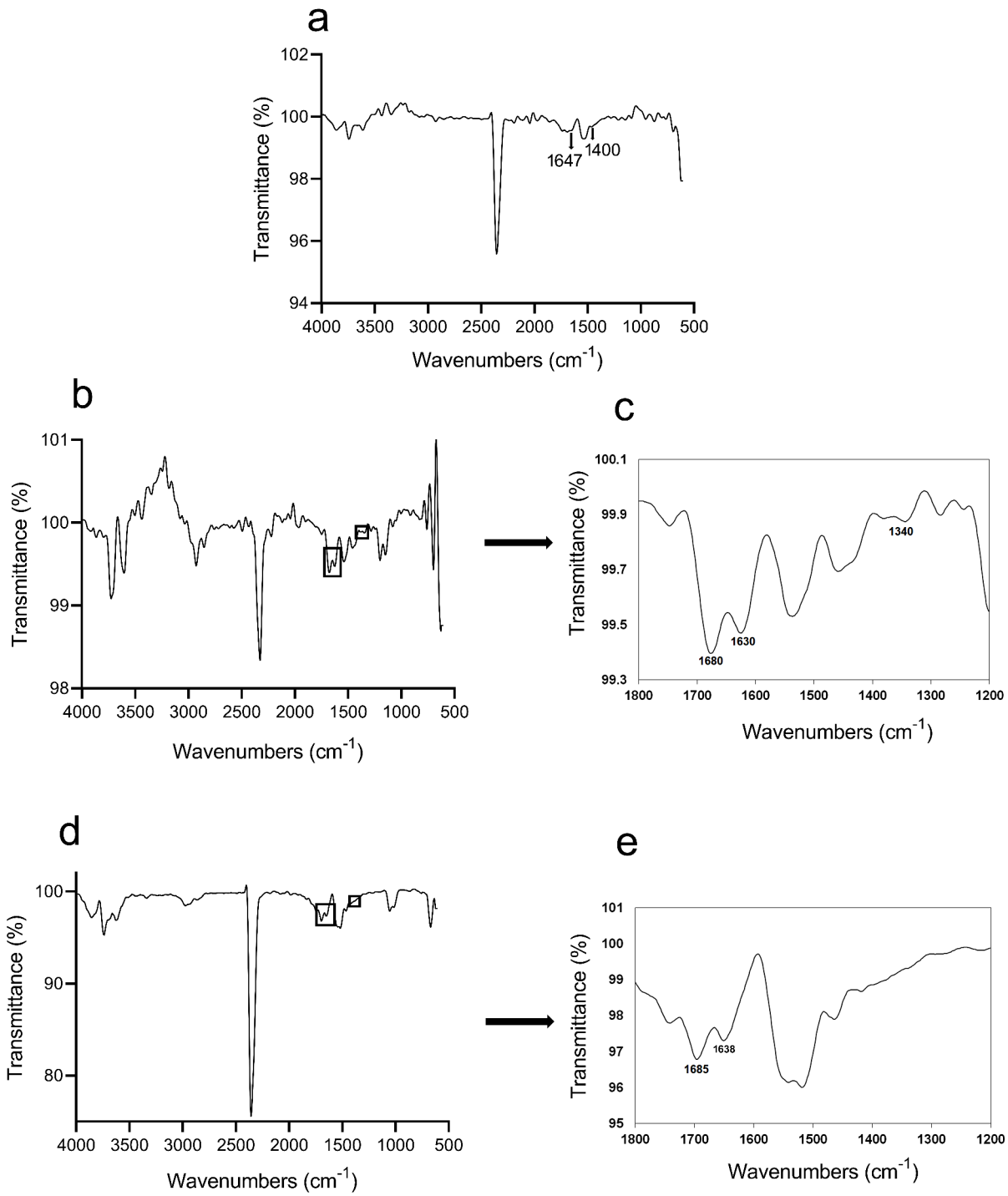

Fig. 3 FTIR spectra of (a) GNP, (b) Pal-α-MSH(11–13) and (d) GNP-Pal-α-MSH(11–13). The boxed regions show the differences and confirm the presence of peptide over the GNP surface. The separated fragments in spectral ranges of 1200 cm^{-1} to 1800 cm^{-1} are shown in (c) Pal-α-MSH(11–13) and (e) GNP-Pal-α-MSH(11–13) for detailed comparison

(~ 10^6 CFU/ml) were incubated with 2 × MIC of GNP-Pal-α-MSH(11–13) (i.e. 36 µM) for 4 h and compared with the treatment of same concentration of Pal-α-MSH(11–13) (equivalent to 3 × MIC) and presented in Fig. 5. The time kill kinetics against stationary phase MSSA cultures showed that at 36 µM concentration, GNP-Pal-α-MSH(11–13)

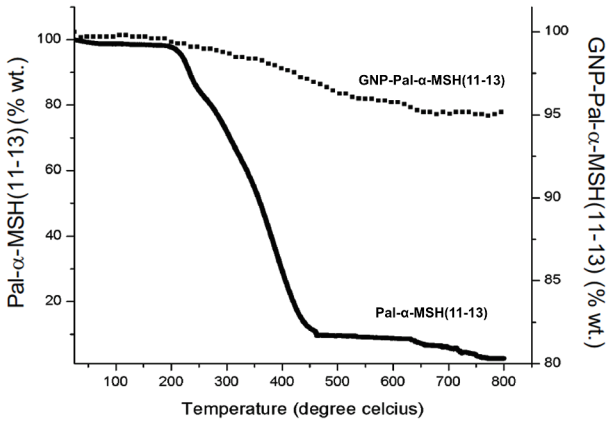

Fig. 4 The thermo-gravimetric analysis (TGA) of Pal-α-MSH(11–13) (continuous line) and GNP-Pal-α-MSH(11–13) (dotted line)

caused 1.8 log reduction after 1 h of incubation, while Pal-α-MSH(11–13) caused a more rapid killing, as shown by 3.6 log reduction within same time (Fig. 5a). Furthermore, the peptide-conjugate increased its bactericidal potency and caused 3.5 log reduction after 2 h, comparable effect was exerted by the peptide alone as shown by 3.7 log reduction. The bactericidal effect was further increased to 4.7 log and 3.9 log reduction by the peptide-conjugate and peptide respectively after 4 h of incubation. Bactericidal efficacy was also observed for stationary phase MRSA cultures, where the GNP-Pal-α-MSH(11–13) caused 3.2 log reduction and the Pal-α-MSH(11–13) exhibited 3.7 log reduction at 36 µM upon 1 h of incubation (Fig. 5b). The peptide alone was able to cause complete eradication of cells after 4 h, while 5.2 log reduction (~99.99% killing) was caused by the peptide-conjugate. The standard antibiotic, vancomycin even at 3 µM (equivalent to 4 × MIC) caused 0.5 log reduction upto 4 h of incubation with both MSSA and MRSA cultures.

In antibacterial study, the stationary phase cells were used as the inoculum and added to fresh TSB, which led to the significant growth in control samples after 24 h. Thus, next, we also determined the efficacy of Pal-α-MSH(11–13) and its GNP conjugate after incubated for 24 h and the data showed that Pal-α-MSH(11–13) was able to completely kill the MSSA cells after 24 h, it's conjugated form caused 5.2 log reduction (~99.99% killing). Vancomycin was able to cause 2.7 log reduction (~99.8% killing) after 24 h of incubation with MSSA and MRSA cells.

Overall, both Pal-α-MSH(11–13) and its conjugate, GNP-Pal-α-MSH(11–13) were successfully able to cause more than 99.9% killing in 4 and 24 h against both MSSA and MRSA cells, thereby ensured their rapid and potent efficacy. The aim of this study was to perform a comparative analysis of rapid antibacterial action of the peptide before and after GNP conjugation and this observation supported the comparable efficacy. Maximum killing effect was exhibited within 4 h of incubation and both peptide and its conjugated form could remain very active even after 24 h. It is also important to mention that bactericidal activity of the peptide and its conjugate were higher than that of vancomycin which is last resort drug for staphylococcal infections.

Biofilm susceptibility

The anti-biofilm potential was also noted by studying the MRSA biofilm inhibition for both Pal-α-MSH(11–13) and its conjugated form. The extent of cell adhesion and cell viability were 7.2 ± 0.24% and 4.26 ± 0.3% for the GNP-Pal-α-MSH(11–13), while the same were 5.44 ± 0.24% and 2.39 ± 0.24% respectively for Pal-α-MSH(11–13) at 36 µM concentration (Fig. 6a and b). The cell survival in biofilm was also determined by scraping and plating the suspensions onto agar. It was observed that the peptide and its conjugate were able to cause 4.4 log and 4 log reduction in the viable cell count of MRSA biofilm (Fig. 6c). As vancomycin

Table 2 Minimal inhibitory concentration (MIC) and minimal bactericidal concentration (MBC) values against MSSA (ATCC 29213) and MRSA (ATCC 33591)

Antimicrobial substances	MSSA (ATCC 29213)			MRSA (ATCC 33591)		
	MIC (µM) (‡ µg/ml)	**MBC (µM)** (‡ µg/ml)	**Tolerance level**	**MIC (µM)** (‡ µg/ml)	**MBC (µM)** (‡ µg/ml)	**Tolerance level**
Pal-α-MSH(11–13)	12 µM ‡ 6.96 µg/ml	12 µM ‡ 6.96 µg/ml	1	12 µM ‡ 6.96 µg/ml	12 µM ‡ 6.96 µg/ml	1
GNP-Pal-α-MSH(11–13) †	18 µM ‡ 10.44 µg/ml	18 µM ‡ 10.44 µg/ml	1	18 µM ‡ 10.44 µg/ml	18 µM ‡ 10.44 µg/ml	1
Vancomycin	0.75 µM ‡ 1.11 µg/ml	1.5 µM ‡ 2.22 µg/ml	2	0.75 µM ‡ 1.11 µg/ml	0.75 µM ‡ 1.11 µg/ml	1

† The MIC or MBC of the GNP-Pal-α-MSH(11–13) represents the concentration of the Pal-α-MSH(11–13) (based on its molecular mass) present in the nanoparticles

‡ Corresponding values in µg/ml

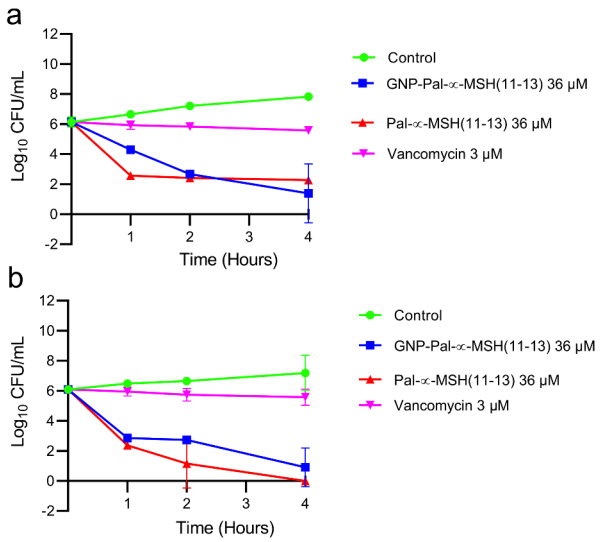

Fig. 5 The antibacterial kinetics against stationary phase cells of (a) MSSA (ATCC 29213) and (b) MRSA (ATCC 33591), after treatment with Pal-α-MSH(11–13), GNP-Pal-α-MSH(11–13) and vancomycin for 4 h. The data represent mean ± standard deviation (SD) for experiments performed twice independently in duplicates

at its 4 × MIC, was unable to exert strong bactericidal activity in killing kinetics study, we used higher concentration of 12 µM (equivalent to 16 × MIC) in biofilm inhibition assays. MRSA biofilm treated with vancomycin exhibited 4.91 ± 0.09% cell adhesion and 2.48 ± 0.05% cell viability (Fig. 6a and b). The antibiotic also caused a reduction of 4.7 log in cell survival of treated biofilm (Fig. 6c).

Hemolysis and cytotoxicity

For hemolysis and cytoxicity assays, the concentration range was extended upto 72 µM for the tested agents, to study their cell selectivity potential at higher concentrations that may be needed to treat other strains. As obtained in the analysis, the peptide conjugation with the GNPs resulted in diminished hemolytic activity against murine RBC (Fig. 7a) as well as cytotoxicity (Fig. 7b) against murine 3T3 fibroblast cells, as evidenced by 0.29 ± 0.03% hemolysis and 100% viable fibroblast cells even at 72 µM compared to the Pal-α-MSH(11–13), which showed 74.99 ± 1.59% hemolysis and 59.39 ± 1.06% viable fibroblasts at said concentration. Comparative analysis with melittin, which is known to possess poor cell selectivity (Dempsey 1990), exhibited 100% hemolysis against murine RBC at 72 µM, while, treatment with triton-X (2%) showed 51.22 ± 0.94% viable murine fibroblasts.

Discussion

The rapid development of antibiotic resistance now-a-days, is leading to the development of alternative strategy of using CAMPs due to their low tendency for resistance development and broad spectrum activity against variety of microorganisms. Over the past decade, Mukhopadhyay and co-researchers have established the α-MSH and their analogues as effective staphylocidal agents (Singh and Mukhopadhyay 2011; Singh et al. 2013, 2016, 2020). Providentially, major limitation of AMPs, like inactivity in presence of bacterial growth media was conquered by the design of N-terminal palmitoylated analogue Pal-α-MSH(11–13), which has been reported to exhibit potent anti-staphylococcal activity against both planktonic cells and biofilm (Mumtaz et al. 2020). Palmitoylation increased the potency against stationary phase cells and also inhibited the biofilm development of both MSSA and MRSA. Similar to the parent peptide, Pal-α-MSH(11–13) was shown to act through membrane permeabilization and rapid depolarization, leading to the cell lysis. However, the palmitoylation resulted in cytotoxicity toward mammalian cells, as evidenced by 50% hemolysis at 62.5 µM and ~ 14.5% killed fibroblast cells at 20 and 50 µM concentrations (Mumtaz et al. 2020). Though the cytotoxic concentration of Pal-α-MSH(11–13) was higher than the bactericidal concentration against the reported strains of MSSA and MRSA, but increasing the potential of cell selectivity at higher concentration is always beneficial for its broad spectrum use against other bacterial strains, where higher MIC may be obtained.

On an aim to reduce the toxicity of Pal-α-MSH(11–13) and to increase its cell selectivity toward mammalian cells, the Pal-α-MSH(11–13) conjugation with GNPs was proposed for the first time in this study. GNPs are highly biocompatible and currently used as drug delivery tools because of the easy surface functionalization and conjugation with other molecules (Cabuzu et al. 2015). Here, GNPs were synthesized using the citrate reduction process, an eminent method that generates nanoparticles of controlled size regulated by optimizing the ratio of the reactants (Frens 1973; Turkevich et al. 1951; Jana et al. 2001; Ghosh and Chattopadhyay 2013). Monodispersed GNPs of 11.94 ± 1.8 nm were obtained in this study, as observed in TEM images. However, Pal-α-MSH(11–13) attachment onto the GNP surfaces resulted in crosslinking the GNPs, thereby forming aggregates, shown in TEM. The particle aggregation may also be confirmed by the higher hydrodynamic diameter of 172.99 ± 15.89 nm of the GNP-Pal-α-MSH(11–13) compared to that of GNPs alone, 23.71 ± 4.21 nm. This was supported by the UV-Vis spectra, where λ_{max} was red shifted from 526 to 632 nm for GNP-Pal-α-MSH(11–13) due to the alteration of surface plasmon resonance of the larger

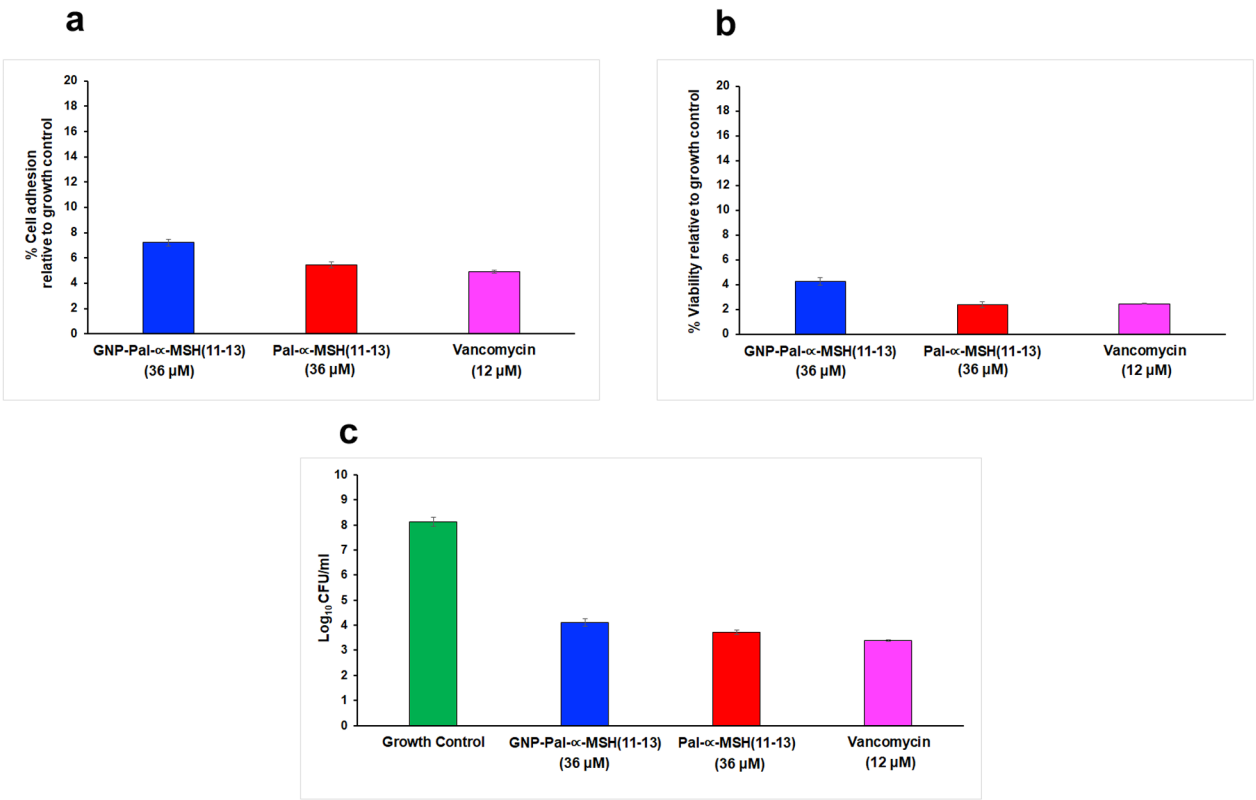

Fig. 6 Inhibition of MRSA (ATCC 33591) biofilm upon treatment with GNP-Pal-α-MSH(11–13) (36 µM), Pal-α-MSH(11–13) (36 µM) and vancomycin (12 µM). (a) % Cell adhesion by the biofilm as determined by the crystal violet (CV) dye binding method, (b) % Viability of the biofilm cells as determined by the MTT assay, (c) Survival of the biofilm cells in $\log_{10}$ CFU/mL as determined by the CFU count assay. The data represent mean ± standard deviation (SD) for experiments performed twice independently in duplicates

particles. Further SAED patterns revealed that the synthesized GNPs and GNP-Pal-α-MSH(11–13), both are crystalline in nature (Singh et al. 2018; Gopinath and Arumugam 2014). The particle aggregation does not always have detrimental effect on their activity, as same phenomenon was also observed by Fuller et al. (2020) and Saha et al. (2007). Despite forming aggregates, the antibiotic conjugated GNPs exhibited better inhibition against bacteria compared to the respective antibiotics only.

Anionic GNPs have strong affinity for thiol (-SH) and amine ($-NH_2$) groups, that allows for their surface functionalization leading to various biomedical and clinical applications (Shukla et al. 2005). The peptide capping over GNPs was supported by our FTIR data. IR absorption peak at 1340 cm^{-1} which is indicative of $-NH_2$ vibration of lysine, appeared in Pal-α-MSH(11–13) spectrum but not in that of GNP-Pal-α-MSH(11–13). Peaks between 1100 and 1200 cm^{-1} of the peptide was also absent in the spectrum of the conjugate, thereby confirmed the reduction and interaction with the free electrons of the $-NH_2$ group. This was corroborative of the results obtained by Bansal et al. (2018), where the authors described a one-step synthesis of GNPs capped with cationic cell penetrating peptide and worked on their intracellular delivery into cancer cells. The spectrum of GNP-Pal-α-MSH(11–13) revealed characteristic peaks of C = O, C-N stretch at 1600–1700 cm^{-1}, also indicated the peptide conjugation over GNP surface (Wangoo et al. 2008). The spectral differences between the peptide and peptide conjugated GNPs confirmed that the peptide-conjugate was formed via electrostatic interaction between anionic $-COO^-$ group on GNPs and cationic $-NH_3^+$ group of lysine residues of peptide.

In Turkevich/ Frens methods, the citrate ions act as reducing agent for GNP synthesis and also stabilize the particles, as confirmed by its highly negative zeta potential of -40.36 mV, obtained in our study. A simple electrostatic interacting strategy was taken to attach the newly reported CAMP, Pal-α-MSH(11–13) onto the surface of negatively charged citrate reduced GNPs. This was also confirmed by the change of zeta value to -26.91 mV for GNP-Pal-α-MSH(11–13), due to the attachment of the cationic peptide. The alteration of zeta potential due to electrostatic conjugation was also observed by Falciani et al. 2020, where a non-natural CAMP, SET-M33 was conjugated with anionic

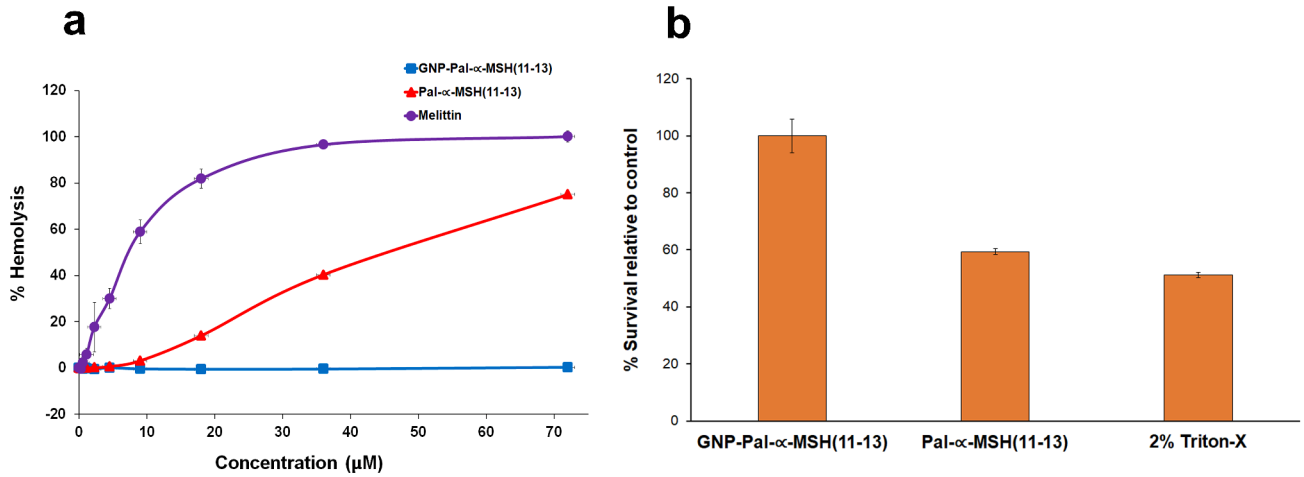

Fig. 7 (a) The percentage hemolysis of mice RBCs upon treatment with GNP-Pal-α-MSH(11–13) (squares), Pal-α-MSH(11–13) (triangles) and melittin (circles) for 1 h. 0.1% Triton X-100 was used as positive control for the experiment. (b) Cytotoxicity of free and conjugated peptides (72 μM) toward the 3T3 murine fibroblast cell line, represented as percentage survival of the cells upon treatment for 2 h relative to the untreated growth control. The data represent mean ± standard deviation (SD) for experiments performed twice independently in duplicates or triplicates

dextran nanoparticles to act against *Pseudomonas aeruginosa*. The zeta potential or surface charge of the molecules play a major role in establishing nano-medicines and their delivery to the target sites. Cationicity of the drug allows strong electrostatic interaction with the negatively charged cells, providing toxicity to both the bacterial and human cells. Therefore, here an aim was to develop overall anionicity in the conjugate by attaching the peptide with GNPs, while not affecting their antibacterial activity significantly. Our result was comparable with the previous report by Salvioni et al. 2017. They developed anionic silver nanoparticles through citrate and tannic acid reduction approach, which exhibited strong antibacterial activity and low cytotoxicity toward eukaryotic cells.

The MIC and MBC of GNP-Pal-α-MSH(11–13) and Pal-α-MSH(11–13) obtained were 18 μM and 12 μM respectively against both MSSA and MRSA strains. The MIC of the peptide-conjugate represented the concentration of the peptide attached onto the GNP surfaces, as the citrate reduced GNPs had no influence on bacterial inhibition up to the tested concentration of 0.15 μM (concentration needed for the synthesis of the conjugate). Previous studies reported that GNPs that were synthesized by plant extracts (MubarakAli et al. 2011; Ahmed et al. 2014) and sodium borohydride (Shamaila et al. 2016) exhibited antimicrobial activity against important pathogens like *Salmonella typhi*, *Klebsiella pneumoniae*, *E. coli* and *S aureus*, whereas, citrate reduced GNPs were reported to have no inhibitory effect as studied by Morales-Avila et al. (2017) and Nur (2013). Zhang et al. (2015) also reviewed that the probable reason behind the antimicrobial activity of GNPs are due to the presence of existing materials like surface functionalizing agents, co-chemicals, gold ions etc. that were not removed completely during the synthesis. In a comparative study by Payne et al. (2016), citrate-GNPs did not exhibit any antibacterial activity, while GNP conjugated with kanamycin antibiotic showed potent activity against *Staphylococcus epidermidis*, *Streptococcus bovis* and *Enterobacter aerogenes*. Therefore, our results were in line with the previous reports of citrate reduced GNPs and their no antibacterial efficacy. In our study, citrate reduction method was preferred not only to impart anionic ($-COO^-$) groups on GNPs but also to prevent some obstacles like lack of purity, polydispersity, poor yield and formation of by-products that may happen during green synthesis approach.

The staphylococcal membrane depolarization and permeabilization of Pal-α-MSH(11–13) has been already established by the previous study of Mumtaz et al. (2020). Electron microscopy images of the MRSA cells treated with the peptide showed alteration of membrane integrity leading to the cell lysis. The membrane depolarizing and permeabilizing potential was also shown to be positively correlated with the anti-staphylococcal efficacy of the peptide. The killing kinetics experiments in our study revealed the comparable pattern of bactericidal action for both Pal-α-MSH(11–13) and GNP-Pal-α-MSH(11–13). Though the peptide showed a more rapid killing in 1 h against MSSA cells, the peptide-conjugate paced up its efficacy and caused 3.5 log reduction in 2 h. The time lag for GNP-Pal-α-MSH(11–13) might account for the time needed to release the peptide from its conjugated form. Encouragingly, upon 24 h of incubation with both MSSA and MRSA cells, both

the treatments caused analogous staphylocidal efficacy. Our observations were in agreement compatible with what was observed for Pal-α-MSH(11–13) previously (Mumtaz et al. 2020). For better understanding, further studies with higher concentrations of the peptide and conjugate against the stationary phase MSSA and MRSA need to be explored in future. The standard antibiotic tested here was vancomycin, a widely used glycopeptide, which exerted a slow killing due to its mechanistic action against cell wall synthesis, achieving 2.7 log reduction upon 24 h of incubation. This was also confirmed by our previous reports (Joshi et al. 2018; Mumtaz et al. 2020) and others (Lopez et al. 2005; McKay et al. 2009).

In our study, the possible mechanism of action of the peptide-conjugate was postulated, though more mechanistic studies will be performed in future for further confirmation. Being the carrier for AMP delivery, the GNPs might release the bound peptides at the target sites, thereby increased the local concentration of the positively charged Pal-α-MSH(11–13) residues to interact efficiently with the negatively charged bacterial membrane, resulting in its perturbation and finally leading to the cell lysis. Several studies also established that, GNP conjugation with cationic peptides did not alter their membrane targeting mechanism and bactericidal efficacy (Casciaro et al. 2017; Luca et al. 2013; Pal et al. 2011). However, further studies are in need to explore the efficiency of peptide release from its bound form followed by its movement and interaction with the target cells. The biofilm formation by MRSA was also noted to be well inhibited by both the peptide and its conjugated form. However, the anti-biofilm potential was slightly higher for Pal-α-MSH(11–13) compared to the peptide-conjugate. This might be expected from the perspective of corresponding MIC values. The standard antibiotic and glycopeptide, vancomycin exerted a comparable efficacy to inhibit the biofilm formation by tested MRSA strain.

Some cationic AMPs exhibit high level of cytotoxicity, that renders them to be less applicable for clinical applications. A potential approach to decrease the AMP toxicity can be feasible via nanofabrication and conjugation with GNPs (Rajchakit and Sarojini 2017). Among the different inorganic nanoparticles, GNPs are considered to be suitable agent as drug loading/carriers because of their stability and biocompatibility (Ghosh et al. 2008). Several factors like shape, size, capping or reducing agents play important roles in determining and diminishing the toxicity of nanoparticles. Connor et al. (2005) reported that spherical GNPs of 18 nm size synthesized with citrate and biotin were found to have no toxicity upto 250 µM, while the precursor gold salt showed 90% toxicity toward leukemia cell line. The high cell selectivity of citrate-GNPs toward dendritic cells was also confirmed by Villiers et al. (2010). Our analysis confirmed a drastic reduction in the hemolytic and cytotoxic profile of Pal-α-MSH(11–13), when conjugated with gold nanoparticles. The peptide-conjugate exerted no hemolysis or fibroblast cytotoxicity upto the tested concentration of 72 µM, thereby established their high cell-selectivity potential. Encouragingly, previous studies also assured the human blood compatibility of citrate-GNPs, as reported by Dobrovolskaia et al. (2009). Our study was in great accordance with the results obtained by Pal et al. (2011). The researchers studied on the antibacterial activity as well as therapeutic potential of some novel cyclic CAMPs and their GNP-conjugated forms. Promisingly, peptide conjugation with GNPs significantly reduced their cytotoxicity without considerably hampering their antimicrobial efficacy.

Conclusions

In conclusion, the current study demonstrates the GNP conjugation with palmitoylated α-MSH(11–13) analogue for the first time. The nano-fabrication was done using tri-sodium citrate as reducing agent and Pal-α-MSH(11–13) analogue as capping agent. An electrostatic interaction strategy was taken to conjugate the citrate reduced anionic GNPs and cationic Pal-α-MSH(11–13). The GNP-Pal-α-MSH(11–13) was nontoxic toward mammalian cells as compared to the unconjugated form, without substantially affecting their bactericidal potency against *S. aureus*. The studies of bactericidal kinetics against MSSA as well as MRSA and inhibition of MRSA biofilm formation indicated the comparable efficacy of the analogue before and after nano-conjugation. Further studies regarding the resistance development and *in vivo* bactericidal potential of the GNP conjugated analogue need to be performed.

Supplementary Information The online version contains supplementary material available at https://doi.org/10.1007/s11274-022-03365-7.

Acknowledgements SM is grateful to DST-SERB for National Post Doctoral Fellowship (File No. PDF/2017/000549). AHM is grateful to CSIR, India for Research Associateship (File No. 09/263(1185)/2019-EMR-I). KM is grateful for receiving funds from DST-SERB (EMR/2016/001708) and DBT (BT/PR27737/MED/29/1265/2018). The authors acknowledge AIRF, JNU, New Delhi, India for TEM analysis and CIF, Jamia Milia Islamia, New Delhi, India for the FTIR analysis. The authors also thank Department of Physics, Jawaharlal Nehru University, New Delhi, India for providing the TGA facility.

Declarations

Conflict of interest The authors declare no conflict of interest in this work.

References

Ahmed KBA, Subramanian S, Sivasubramanian A, Veerappan G, Veerappan A (2014) Preparation of gold nanoparticles using *Salicornia brachiata* plant extract and evaluation of catalytic and antibacterial activity. Spectrochim Acta 130:54–58. https://doi.org/10.1016/j.saa.2014.03.070

Bansal K, Aqdas M, Kumar M, Bala R, Singh S, Agrewala JN, Katare OP, Sharma RK, Wangoo N (2018) A facile approach for synthesis and intracellular delivery of size tunable cationic peptide functionalized gold nanohybrids in cancer cells. Bioconjug Chem 29:1102–1110. https://doi.org/10.1021/acs.bioconjchem.7b00772

Baptista P, Doria G, Henriques D, Pereira E, Franco R (2005) Colorimetric detection of eukaryotic gene expression with DNA-derivatized gold nanoparticles. J Biotech 119:111–117. https://doi.org/10.1016/j.jbiotec.2005.02.019

Bonor J, Reddy V, Akkiraju H, Dhurjati P, Nohe A (2014) Synthesis and characterization of L-Lysine conjugated silver nanoparticles smaller than 10 nM. Adv Sci Eng Med 6:942–947. https://doi.org/10.1166/asem.2014.1583

Cabuzu D, Cirja A, Puiu R, Grumezescu AM (2015) Biomedical applications of gold nanoparticles. Curr Top Med Chem 15:1605–1613. https://doi.org/10.2174/1568026615666150414144750

Casciaro B, Moros M, Rivera-Fernandez S, Bellelli A, de la Fuente JM, Luisa Mangoni M (2017) Gold-nanoparticles coated with the antimicrobial peptide esculentin-1a(1–21)NH_2 as a reliable strategy for antipseudomonal drugs. Acta Biomater 47:170–181. https://doi.org/10.1016/j.actbio.2016.09.041

Catania A, Grieco P, Randazzo A, Novellino E, Gatti S, Rossi C, Colombo G, Lipton JM (2005) Three-dimensional structure of the alpha-MSH-derived candidacidal peptide $[Ac\text{-}CKPV]_2$. J Pept Res 66:19–26. https://doi.org/10.1111/j.1399-3011.2005.00265.x

Chambers HF, Deleo FR (2009) Waves of resistance: *Staphylococcus aureus* in the antibiotic era. Nat Rev Microbiol 7:629–641. https://doi.org/10.1038/nrmicro2200

Charnley M, Moir AJG, Douglas CWI, Haycock JW (2008) Antimicrobial action of melanocortin peptides and identification of a novel X-Pro-D/L-Val sequence in Gram-positive and Gram-negative bacteria. Peptides 29:1004–1009. https://doi.org/10.1016/j.peptides.2008.02.004

Clinical and Laboratory Standards Institute, CLSI (2018) Performance Standards for Antimicrobial Susceptibility Testing (28th ed) CLSI supplement M100. Wayne, PA

Connor EE, Mwamuka J, Gole A, Murphy CJ, Wyatt MD (2005) Gold nanoparticles are taken up by human cells but do not cause acute cytotoxicity. Small 1:325–327. https://doi.org/10.1002/smll.200400093

Dempsey CE (1990) The actions of melittin on membranes. Biochim Biophys Acta 1031:143–161. https://doi.org/10.1016/0304-4157(90)90006-x

Dobrovolskaia MA, Patri AK, Zheng J, Clogston JD, Ayub N, Aggarwal P, Neun BW, Hall JB, McNeil SE (2009) Interaction of colloidal gold nanoparticles with human blood: effects on particle size and analysis of plasma protein binding profiles. Nanomed 5:106–117. https://doi.org/10.1016/j.nano.2008.08.001

Falciani C, Zevolini F, Brunetti J, Riolo G, Gracia R, Marradi M, Loinaz I, Ziemann C, Cossío U, Llop J, Bracci L, Pini A (2020) Antimicrobial peptide-loaded nanoparticles as inhalation therapy for *Pseudomonas aeruginosa* infections. Int J Nanomed 15:1117–1128. https://doi.org/10.2147/IJN.S218966

Ferri M, Ranucci E, Romagnoli P, Giaccone V (2017) Antimicrobial resistance: A global emerging threat to public health systems. Crit Rev Food Sci Nutr 57:2857–2876. https://doi.org/10.1080/10408398.2015.1077192

Frens G (1973) Controlled nucleation for the regulation of the particle size in monodisperse gold suspensions. Nat Phys Sci 241:20–22. https://doi.org/10.1038/physci241020a0

Fuller M, Whiley H, Köper I (2020) Antibiotic delivery using gold nanoparticles. SN Appl Sci 2:1022. https://doi.org/10.1007/s42452-020-2835-8

Ghosh D, Chattopadhyay N (2013) Gold nanoparticles: Acceptors for efficient energy transfer from the photoexcited fluorophores. Opt Photonics J 3:18–26. https://doi.org/10.4236/opj.2013.31004

Ghosh P, Han G, De M, Kim CK, Rotello VM (2008) Gold nanoparticles in delivery applications. Adv Drug Deliv Rev 60:1307–1315. https://doi.org/10.1016/j.addr.2008.03.016

Gopinath K, Arumugam A (2014) Extracellular mycosynthesis of gold nanoparticles using *Fusarium solani*. Appl Nanosci 4:657–662. https://doi.org/10.1007/s13204-013-0247-4

Grieco P, Carotenuto A, Auriemma L, Limatola A, Di Maro S, Merlino F, Mangoni ML, Luca V, Di Grazia A, Gatti S, Campiglia P, Gomez-Monterrey I, Novellino E, Catania A (2013) Novel α-MSH peptide analogues with broad spectrum antimicrobial activity. PLoS ONE 8:e61614. https://doi.org/10.1371/journal.pone.0061614

Hall JB, Dobrovolskaia MA, Patri AK, McNeil SE (2007) Characterization of nanoparticles for therapeutics. Nanomed (Lond) 2:789–803. https://doi.org/10.2217/17435889.2.6.789

Huan Y, Kong Q, Mou H, Yi H (2020) Antimicrobial peptides: classification, design, application and research progress in multiple fields. Front Microbiol 11:582779. https://doi.org/10.3389/fmicb.2020.582779

Jana NR, Gearheart L, Murphy CJ (2001) Seeding growth for size control of 5–40 nm diameter gold nanoparticle. Langmuir 17:6782–6786. https://doi.org/10.1021/la0104323

Joshi S, Mumtaz S, Singh J, Pasha S, Mukhopadhyay K (2018) Novel miniature membrane active lipopeptidomimetics against planktonic and biofilm embedded methicillin-resistant *Staphylococcus aureus*. Sci Rep 8:1021. https://doi.org/10.1038/s41598-017-17234-z

Lee B, Park J, Ryu M, Kim S, Joo M, Yeom JH, Kim S, Park Y, Lee K, Bae J (2017) Antimicrobial peptide-loaded gold nanoparticle-DNA aptamer conjugates as highly effective antibacterial therapeutics against *Vibrio vulnificus*. Sci Rep 7:13572. https://doi.org/10.1038/s41598-017-14127-z

Lister JL, Horswill AR (2014) *Staphylococcus aureus* biofilms: recent developments in biofilm dispersal. Front Cell Infect Microbiol 4:178. https://doi.org/10.3389/fcimb.2014.00178

Lopez S, Hackbarth C, Romanò G, Trias J, Jabes D, Goldstein BP (2005) In vitro antistaphylococcal activity of dalbavancin, a novel glycopeptide. J Antimicrob Chemother 55 Suppl 2:ii21–ii24. https://doi.org/10.1093/jac/dki007

Luca V, Stringaro A, Colone M, Pini A, Mangoni ML (2013) Esculentin(1–21), an amphibian skin membrane-active peptide with potent activity on both planktonic and biofilm cells of the bacterial pathogen *Pseudomonas aeruginosa*. Cell Mol Life Sci 70:2773–2786. https://doi.org/10.1007/s00018-013-1291-7

Mahlapuu M, Håkansson J, Ringstad L, Björn C (2016) Antimicrobial peptides: An emerging category of therapeutic agents. Front Cell Infect Microbiol 6:194. https://doi.org/10.3389/fcimb.2016.00194

Manohar P, Loh B, Athira S, Nachimuthu R, Hua X, Welburn SC, Leptihn S (2020) Secondary bacterial Infections during pulmonary viral disease: Phage therapeutics as alternatives to antibiotics? Front Microbiol 11:1434. https://doi.org/10.3389/fmicb.2020.01434

Manson J, Kumar D, Meenan BJ, Dixon D (2011) Polyethylene glycol functionalized gold nanoparticles: the influence of capping density on stability in various media. Gold Bull 44:99–105. https://doi.org/10.1007/s13404-011-0015-8

May J, Shannon K, King A, French G (1998) Glycopeptide tolerance in *Staphylococcus aureus*. J Antimicrob Chemother 42:189–197. https://doi.org/10.1093/jac/42.2.189

McKay GA, Beaulieu S, Arhin FF, Belley A, Sarmiento I, Parr T Jr, Moeck G (2009) Time-kill kinetics of oritavancin and comparator agents against *Staphylococcus aureus*, *Enterococcus faecalis* and *Enterococcus faecium*. J Antimicrob Chemother 63:1191–1199. https://doi.org/10.1093/jac/dkp126

Mohammed AE, Al-Qahtani A, Al-Mutairi A, Al-Shamri B, Aabed KF (2018) Antibacterial and cytotoxic potential of biosynthesized silver nanoparticles by some plant extracts. Nanomaterials (Basel) 8:382. https://doi.org/10.3390/nano8060382

Mondal AH, Yadav D, Mitra S, Mukhopadhyay K (2020) Biosynthesis of silver nanoparticles using culture supernatant of *Shewanella* sp. ARY1 and their antibacterial activity. Int J Nanomed 15:8295–8310. https://doi.org/10.2147/IJN.S274535

Morales-Avila E, Ferro-Flores G, Ocampo-García BE, López-Téllez G, López-Ortega J, Rogel-Ayala DG, Sánchez-Padilla D (2017) Antibacterial efficacy of gold and silver nanoparticles functionalized with the Ubiquicidin (29–41) antimicrobial peptide. J Nanomater 2017:5831959. https://doi.org/10.1155/2017/5831959

MubarakAli D, Thajuddin N, Jeganathan K, Gunasekaran M (2011) Plant extract mediated synthesis of silver and gold nanoparticles and its antibacterial activity against clinically isolated pathogens. Colloids Surf B Biointerfaces 85:360–365. https://doi.org/10.1016/j.colsurfb.2011.03.009

Mumtaz S, Behera S, Mukhopadhyay K (2020) Lipidated short analogue of α-melanocyte stimulating hormone exerts bactericidal activity against the stationary phase of methicillin-resistant *Staphylococcus aureus* and inhibits biofilm formation. ACS Omega 5:28425–28440. https://doi.org/10.1021/acsomega.0c01462

Nur Y(2013) Gold nanoparticles: Synthesis, characterisation and their effect on *Pseudomonas fluorescens*. Thesis, School of Geography, Earth and Environmental Sciences, The University of Birmingham

Pal S, Mitra K, Azmi S, Ghosh JK, Chakraborty TK (2011) Towards the synthesis of sugar amino acid containing antimicrobial non-cytotoxic CAP conjugates with gold nanoparticles and a mechanistic study of cell disruption. Org Biomol Chem 9:4806–4810. https://doi.org/10.1039/C1OB05338H

Payne JN, Waghwani HK, Connor MG, Hamilton W, Tockstein S, Moolani H, Chavda F, Badwaik V, Lawrenz MB, Dakshinamurthy R (2016) Novel synthesis of kanamycin conjugated gold nanoparticles with potent antibacterial activity. Front Microbiol 7:607. https://doi.org/10.3389/fmicb.2016.00607

Rajchakit U, Sarojini V (2017) Recent developments in antimicrobial-peptide-conjugated gold nanoparticles. Bioconjug Chem 28:2673–2686. https://doi.org/10.1021/acs.bioconjchem.7b00368

Saha B, Bhattacharya J, Mukherjee A, Ghosh A, Santra C, Dasgupta AK, Karmakar P (2007) In vitro structural and functional evaluation of gold nanoparticles conjugated antibiotics. Nanoscale Res Lett 2:614–622. https://doi.org/10.1007/s11671-007-9104-2

Salvioni L, Galbiati E, Collico V, Alessio G, Avvakumova S, Corsi F, Tortora P, Prosperi D, Colombo M (2017) Negatively charged silver nanoparticles with potent antibacterial activity and reduced toxicity for pharmaceutical preparations. Int J Nanomed 12:2517–2530. https://doi.org/10.2147/IJN.S127799

Shamaila S, Zafar N, Riaz S, Sharif R, Nazir J, Naseem S (2016) Gold nanoparticles: An efficient antimicrobial agent against enteric bacterial human pathogen. Nanomaterials (Basel) 6:71. https://doi.org/10.3390/nano6040071

Shireen T, Singh M, Dhawan B, Mukhopadhyay K (2012) Characterization of cell membrane parameters of clinical isolates of *Staphylococcus aureus* with varied susceptibility to alpha-melanocyte stimulating hormone. Peptides 37:334–339. https://doi.org/10.1016/j.peptides.2012.05.025

Shukla R, Bansal V, Chaudhary M, Basu A, Bhonde RR, Sastry M (2005) Biocompatibility of gold nanoparticles and their endocytotic fate inside the cellular compartment: A microscopic overview. Langmuir 21:10644–10654. https://doi.org/10.1021/la0513712

Singh H, Du J, Singh P, Yi TH (2018) Ecofriendly synthesis of silver and gold nanoparticles by *Euphrasia officinalis* leaf extract and its biomedical applications. Artif Cells Nanomed Biotechnol 46:1163–1170. https://doi.org/10.1080/21691401.2017.1362417

Singh J, Joshi S, Mumtaz S, Maurya N, Ghosh I, Khanna S, Natarajan VT, Mukhopadhyay K (2016) Enhanced cationic charge is a key factor in promoting Staphylocidal activity of α-melanocyte stimulating hormone via selective lipid affinity. Sci Rep 6:31492. https://doi.org/10.1038/srep31492

Singh J, Mumtaz S, Joshi S, Mukhopadhyay K (2020) In Vitro and Ex Vivo Efficacy of Novel Trp-Arg Rich Analogue of α-MSH against *Staphylococcus aureus*. ACS Omega 5:3258–3270. https://doi.org/10.1021/acsomega.9b03307

Singh M, Gadepalli R, Dhawan B, Mukhopadhyay K (2013) Combination of alpha-melanocyte stimulating hormone with conventional antibiotics against methicillin resistant *Staphylococcus aureus*. PLoS ONE 8:e73815. https://doi.org/10.1371/journal.pone.0073815

Singh M, Mukhopadhyay K (2011) C-terminal amino acids of alpha-melanocyte-stimulating hormone are requisite for its antibacterial activity against *Staphylococcus aureus*. Antimicrob Agents Chemother 55:1920–1929. https://doi.org/10.1128/AAC.00957-10

Singh M, Mukhopadhyay K (2014) Alpha-Melanocyte Stimulating Hormone: An emerging anti-inflammatory antimicrobial peptide. BioMed Res Int 874610. https://doi.org/10.1155/2014/874610

Singh R, Patil S, Singh N, Gupta S (2017) Dual functionality nanobioconjugates targeting intracellular bacteria in cancer cells with enhanced antimicrobial activity. Sci Rep 7:5792. https://doi.org/10.1038/s41598-017-06014-4

Suvarna S, Das U, KC S, Mishra S, Sudarshan M, Saha KD, Dey S, Chakraborty A, Narayana Y (2017) Synthesis of a novel glucose capped gold nanoparticle as a better theranostic candidate. PLoS ONE 12:e0178202. https://doi.org/10.1371/journal.pone.0178202

Tiwari K, Singh M, Kumar P, Mukhopadhyay K(2022) Binding of cationic analogues of α-MSH to lipopolysaccharide and disruption of the cytoplasmic membranes caused bactericidal action against *Escherichia coli*. Sci Rep. 12:1987. https://doi.org/10.1038/s41598-022-05684-z

Tong SYC, Davis JS, Eichenberger E, Holland TL, Fowler VG Jr (2015) *Staphylococcus aureus* infections: epidemiology, pathophysiology, clinical manifestations, and management. Clin Microbiol Rev 28:603–661. https://doi.org/10.1128/CMR.00134-14

Traba C, Liang JF (2011) Susceptibility of *Staphylococcus aureus* biofilms to reactive discharge gases. Biofouling 27:763–772. https://doi.org/10.1080/08927014.2011.602188

Trautner BW, Darouiche RO (2004) Catheter-associated infections: pathogenesis affects prevention. Arch Intern Med 164:842–850. https://doi.org/10.1001/archinte.164.8.842

Turkevich J, Stevenson PC, Hillier J (1951) A study of the nucleation and growth processes in the synthesis of colloidal gold. Discuss Faraday Soc 11:55–75. https://doi.org/10.1039/DF9511100055

Villiers C, Freitas H, Couderc R, Villiers MB, Marche PN (2010) Analysis of the toxicity of gold nanoparticles on the immune system: effect on dendritic cell functions. J Nanopart Res 12:55–60. https://doi.org/10.1007/s11051-009-9692-0

Wangoo N, Bhasin KK, Mehta SK, Suri CR (2008) Synthesis and capping of water-dispersed gold nanoparticles by an amino acid: bioconjugation and binding studies. J Colloid Interface Sci 323:247–254. https://doi.org/10.1016/j.jcis.2008.04.043

Yeom JH, Lee B, Kim D, Lee JK, Kim S, Bae J, Park Y, Lee K (2016) Gold nanoparticle-DNA aptamer conjugate-assisted delivery of antimicrobial peptide effectively eliminates intracellular *Salmonella enterica serovar Typhimurium*. Biomaterials 104:43–51. https://doi.org/10.1016/j.biomaterials.2016.07.009

Yougbare S, Chang TK, Tan SH, Kuo JC, Hsu PH, Su CY, Kuo TR (2019) Antimicrobial gold nanoclusters: Recent developments and future perspectives. Int J Mol Sci 20:2924. https://doi.org/10.3390/ijms20122924

Zhang Y, ShareenaDasari TP, Deng H, Yu H (2015) Antimicrobial activity of gold nanoparticles and ionic gold. J Environ Sci Health C Environ Carcinog Ecotoxicol Rev 33:286–327. https://doi.org/10.1080/10590501.2015.1055161